

THE COLORS OF EXTREME OUTER SOLAR SYSTEM OBJECTS

SCOTT S. SHEPPARD

Department of Terrestrial Magnetism, Carnegie Institution of Washington, 5241 Broad Branch Rd. NW, Washington, DC 20015, USA; sheppard@dtm.ciw.edu
Received 2009 September 24; accepted 2010 January 26; published 2010 March 4

ABSTRACT

Extreme outer solar system objects have possible origins beyond the Kuiper Belt edge, high inclinations, very large semimajor axes, or large perihelion distances. Thirty-three such objects were observed in this work to determine their optical colors. All three objects that have been dynamically linked to the inner Oort Cloud by various authors ((90377) Sedna, 2006 SQ₃₇₂, and (87269) 2000 OO₆₇) were found to have ultra-red surface material (spectral gradient, $S \sim 25$). Ultra-red material is generally associated with rich organics and the low inclination “cold” classical Kuiper Belt objects (KBOs). The observations detailed here show that very red material may be a more general feature for objects kept far from the Sun. The recently discovered retrograde outer solar system objects (2008 KV₄₂ and 2008 YB₃) and the high inclination object (127546) 2002 XU₉₃ show only moderately red surfaces ($S \sim 9$) very similar to known comets, suspected dead comets, Jupiter and Neptune Trojans, irregular satellites, D-type asteroids, and damocloids. The extended or detached disk objects, which have large perihelion distances and are thus considered to be detached from the influence of the giant planets but yet have large eccentricities, are found to have mostly moderately red colors ($10 \lesssim S \lesssim 18$). The colors of the detached disk objects, including the dynamically unusual 2004 XR₁₉₀ and (148209) 2000 CR₁₀₅, are similar to the scattered disk and Plutino populations. Thus the detached disk, scattered disk, Plutino, and high inclination “hot” classical objects likely have a similar mix of objects from the same source regions. Outer classical KBOs, including (48639) 1995 TL₈, were found to have very red surfaces ($18 \lesssim S \lesssim 30$). The low inclination “cold” classical KBOs, outer classical KBOs and possibly the inner Oort Cloud appear to be dominated by ultra-red objects ($S \gtrsim 25$) and thus do not likely have a similar mix of objects as the other outer solar system reservoirs such as the scattered disk, detached disk, and Trojan populations. A possible trend was found for the detached disk and outer classical Kuiper Belt in that objects with smaller eccentricities have redder surfaces irrespective of inclinations or perihelion distances. There is also a clear trend that objects more distant appear redder.

Key words: comets: general – Kuiper Belt: general – minor planets, asteroids: general – Oort Cloud – planets and satellites: formation

Online-only material: color figures

1. INTRODUCTION

The dynamical and physical properties of small bodies in our solar system offer one of the few constraints on the formation, evolution, and migration of the planets. The Kuiper Belt has been found to be dynamically structured with several observed dynamical classes (Trujillo et al. 2001; Kavelaars et al. 2008, 2009); see Figure 1. Classical Kuiper Belt objects (KBOs) have semimajor axes $42 \lesssim a \lesssim 48$ AU with moderate eccentricities ($e \sim 0.1$) and inclinations. These objects may be regarded as the population originally predicted for the Kuiper Belt, but their relatively large eccentricities and inclinations were unexpected. The dynamics of the classical KBOs have shown that the outer solar system has been highly modified through the evolution of the solar system (Duncan & Levison 1997; Petit et al. 1999; Ida et al. 2000; Morbidelli & Levison 2004; Gomes et al. 2005). Resonant KBOs are in mean motion resonances with Neptune and generally have higher eccentricities and inclinations than classical KBOs. These objects, which include Pluto and the Plutinos in the 3:2 resonance, were likely captured into these resonances from the outward migration of Neptune (Malhotra 1995; Hahn & Malhotra 2005; Levison et al. 2008). Scattered disk objects have large eccentricities with perihelia near the orbit of Neptune ($q \sim 25$ –35 AU). The scattered disk objects are likely to have been scattered into their current orbits through interactions with Neptune (Duncan & Levison 1997; Duncan 2008a; Gomes et al. 2008).

A new class of outer solar system object, called the extended or detached disk (Figure 1), has only recently been recognized (Gladman et al. 2002; Emel’yanenko et al. 2003; Morbidelli & Levison 2004; Allen et al. 2006). To date only a few detached disk objects are known. The detached disk objects have large eccentricities, but unlike the scattered disk objects the detached disk objects have perihelia $q \gtrsim 38$ AU, which do not appear to be directly caused by Neptune interactions alone (Gladman & Collin 2006; Levison et al. 2008). Though unexpected, the discovery of these detached disk objects have given us a new understanding of our solar system’s chaotic history.

A few objects have been found that have very large semimajor axes and eccentricities (Sedna, 2006 SQ₃₇₂, and 2000 OO₆₇). Through dynamical simulations these objects are best described as coming from the inner Oort Cloud (Brown et al. 2004; Kenyon & Bromley 2004; Morbidelli & Levison 2004; Kaib et al. 2009). Two objects have also been found to have retrograde orbits in the outer solar system (2008 KV₄₂ and 2008 YB₃). These two retrograde objects along with the very high inclination object 2002 XU₉₃ ($i \sim 78^\circ$) could be from the outer Oort Cloud or a possibly yet to be discovered high inclination source region (Gladman et al. 2009).

Some trans-Neptunian objects (TNOs) have likely not experienced significant thermal evolution since their formation. The amount of thermal evolution depends on how close the object formed to the Sun and how close it has approached the Sun during its lifetime (Meech et al. 2009). The objects in the Kuiper

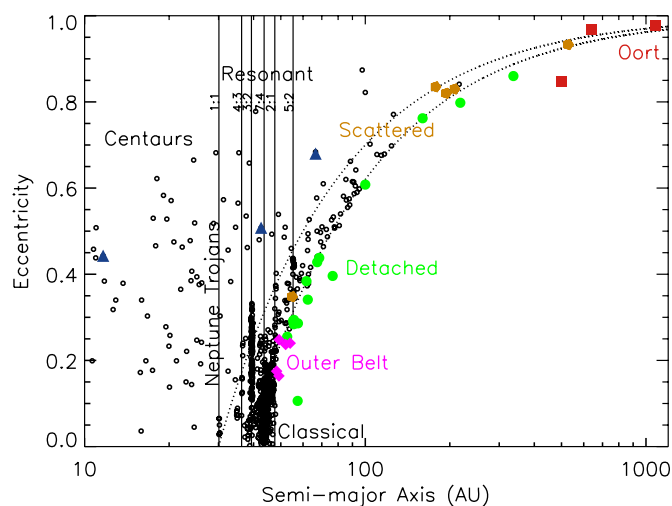


Figure 1. Semimajor axis vs. eccentricity of multi-opposition observed TNOs. This figure shows several distinct dynamical KBO populations. Vertical solid lines show resonances with Neptune as well as the Neptune Trojans in the 1:1 resonance. Scattered disk objects have perihelia $30 \lesssim q \lesssim 38$ AU which are shown by dashed lines. Classical objects are in the lower center portion of the figure. An edge around 48 AU can clearly be seen for low eccentricity objects. Centaurs are on unstable orbits between the giant planets. The objects observed in this work are shown by filled symbols: Inner Oort cloud objects (red squares), extended or detached disk objects (green circles), outer classical belt objects (purple diamonds), retrograde and high inclination objects (blue triangles), extreme scattered disk objects (brown pentagons).

Belt dynamical classes had varied histories with some experiencing very little thermal evolution, making them some of the most primitive bodies in the solar system. Optical observations of TNOs and Centaurs have shown some of these objects have the reddest material known in the solar system (Figure 2; Jewitt & Luu 2001; Peixinho et al. 2004; Doressoundiram et al. 2008; Tegler et al. 2008). This ultra-red material is currently thought to be rich in organic material (Gradie & Veverka 1980; Vilas & Smith 1985; Cruikshank et al. 2005; de Bergh et al. 2008). The ultra-red color may be from Triton tholins and ice tholins, which can be produced by bombarding simple organic ice mixtures with ionizing radiation (Doressoundiram et al. 2003; Barucci et al. 2005a; Emery et al. 2007; Barucci et al. 2008).

Interestingly, short-period comets that are believed to have originated from the Kuiper Belt do not show this ultra-red material (Figure 2; Jewitt 2002). The reason is because comet surfaces have been highly processed from their relatively close passages to the Sun (Jewitt 2002; Grundy 2009). This demonstrates that the surfaces of comets are not reliable for understanding the original compositions of the comets. Some Centaurs, which are the precursors to the short-period comets, do show these ultra-red colors probably because they have not yet been near the Sun for a long enough time to have their surfaces highly modified from thermal, sublimation, or evaporation processes. No long-period comets from the Oort Cloud have been sufficiently observed before any significant heating would have taken place on their surfaces. Thus we do not have a good knowledge of what color an Oort Cloud comet may have been before it started to thermally evolve (Meech et al. 2009).

There have been one or possibly two subsets of TNOs that appear to be dominated by the ultra-red material (Figure 2). First are the low inclination “cold” classical KBOs that also have large perihelions (Tegler & Romanishin 2000; Trujillo & Brown 2002; Doressoundiram et al. 2005; Gulbis et al. 2006; Fulchignoni et al. 2008; Peixinho et al. 2008). These

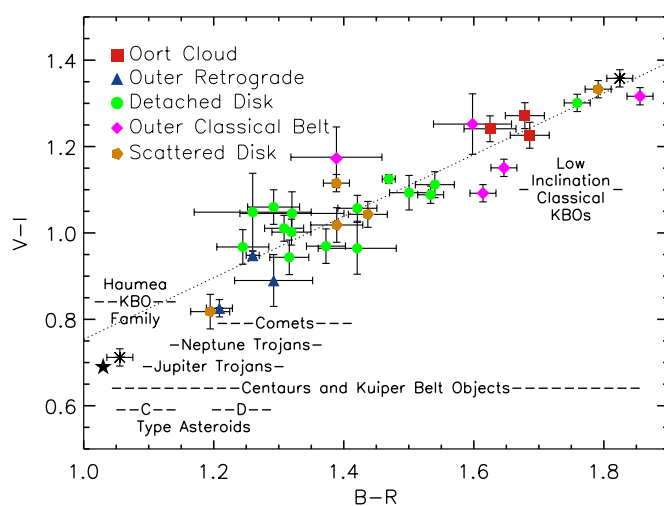


Figure 2. New $B - R$ and $V - I$ colors for objects observed in our sample. The possible inner Oort Cloud objects (red squares) are all near the ultra-red portion of the figure and are similar to the color of low inclination classical KBOs. The outer retrograde and high inclination objects (blue triangles) are slightly red and similar to the colors of the comets, Jupiter Trojans and Neptune Trojans. The extended or detached disk objects (green circles) occupy a fairly large range from moderately red to near but mostly less than ultra-red. The outer classical belt objects (purple diamonds) are mostly near the ultra-red area. Various extreme scattered disk objects observed in this work are also shown (brown pentagons). For reference, the color of the Sun is marked by a filled black star. The very neutral colored Haumea collisional family member 1996 TO₆₆ and the extremely ultra-red object 1999 OX₃ (X’s) were observed to show the large range of known colors in the outer solar system and confirm the photometry results. Also shown are the typical $B - R$ colors found for the C- and D-type asteroids, Jupiter Trojans, Neptune Trojans, comets, Haumea collisional family members, low inclination classical KBOs, Centaurs, and KBOs. The typical colors of all these objects are generally at the same level and slope as shown by the dotted line. The ultra-red material only seen on some KBOs and Centaurs are shown in the upper right. Moderately red objects like the Trojans, comets, and some KBOs and Centaurs can be seen in the middle left of the figure. Gray or neutral colored objects like most main belt asteroids are in the lower left of the figure. There is an obvious trend that more distant objects appear to show redder colors. A $B - R$ color $\gtrsim 1.6$ or $V - I$ color $\gtrsim 1.2$ mag indicates ultra-red color (based on including the reddest 90% of the low inclination classical KBOs).

objects likely formed in the more distant solar system unlike the higher inclination KBOs, which may have formed closer to the Sun and were transported to and captured in the Kuiper Belt during the planet migration process (Levison & Morbidelli 2003; Gomes 2003; Levison et al. 2008). Sedna, an object well beyond the Kuiper Belt edge at 50 AU (Jewitt et al. 1998; Allen et al. 2001), also has an ultra-red color and could be a new class of object, possibly from the inner Oort Cloud (Brown et al. 2004; Morbidelli & Levison 2004; Kenyon & Bromley 2004; Brasser et al. 2006; Barucci et al. 2005b). Some previous works (Tegler & Romanishin 2000; Trujillo & Brown 2002; Doressoundiram et al. 2005) have noted that objects with larger perihelion distances tend to have redder surfaces, but most of the ultra-red objects observed were in the main classical Kuiper Belt. No systematic survey of the colors of the large perihelion detached disk population has been performed to date.

In this work, the optical colors were observed for most of the known detached disk objects, possible inner Oort Cloud objects, and other outer solar system objects that exhibit extreme orbits in terms of their inclination, semimajor axis, or perihelion distance. Understanding any color trends or correlations, in particular the ultra-red material, will constrain where these extreme objects may have formed in the solar system and thus how they may have ended up on their current orbits. This in turn will allow

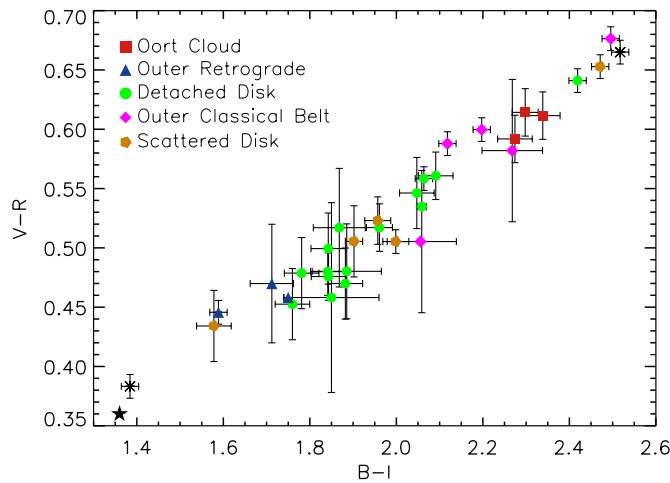


Figure 3. Same as Figure 2 except for $B - I$ and $V - R$ colors. Colors with $B - I \gtrsim 2.2$, $V - R \gtrsim 0.6$, or $R - I \gtrsim 0.6$ mag indicate ultra-red colors (based on including the reddest 90% of the low inclination classical KBOs).

(A color version of this figure is available in the online journal.)

us to determine how the planets may have migrated and what amount of this ultra-red organic-rich material may have been incorporated into the planets.

2. OBSERVATIONS AND ANALYSIS

Observations of the outer solar system objects presented in this work were obtained with the twin Magellan Baade and Clay 6.5 m telescopes at Las Campanas, Chile and the 8.2 m Subaru telescope atop Mauna Kea in Hawaii. Table 1 shows the various observational circumstances for the 33 objects observed. The LDSS3 camera on the Clay telescope was used on the nights of 2005 November 2 and 3, 2008 May 7 and 8, 2009 January 28, 2009 May 23 and 24, and 2009 August 25 and 26. LDSS3 is a CCD imager with one STA0500A 4064×4064 CCD and $15 \mu\text{m}$ pixels. The field of view is about 8.3 arcmin in diameter with a scale of 0.189 arcsec per pixel. The IMACS camera on the Baade telescope was used on the nights of 2008 October 19 and 2008 December 3. IMACS is a wide-field CCD imager that has eight 2048×4096 pixel CCDs with a pixel scale of 0.20 arcsec per pixel. The eight CCDs are arranged in a box pattern with four above and four below and about 12 arcsec gaps between chips. Only chip 2, which is just north and west of the camera center, was used in the IMACS color analysis. The Suprime-Cam imager on the Subaru telescope was used on the night of 2009 October 15. Suprime-Cam is a wide-field CCD imager that has ten 2048×4096 pixel CCDs with a pixel scale of 0.20 arcsec per pixel (Miyazaki et al. 2002). The 10 CCDs are arranged in a 5×2 box pattern similar to the IMACS imager. Only chip 5, which is just west of the camera center, was used in the Suprime-Cam color analysis.

Dithered twilight flat fields and biases were used to reduce each image. Images were acquired through either the Sloan g' , r' , or i' filter while the telescope was auto-guiding at sidereal rates using nearby bright stars. Exposure times were between 300 s and 450 s. Southern Sloan standard stars were used to photometrically calibrate the data (Smith et al. 2005). In order to more directly compare our results with previous works, the Sloan colors were converted to the Johnson–Morgan–Cousins $BVRI$ color system using transfer equations from Smith et al. (2002). To verify the color transformation, the known ultra-red (44594) 1999 OX₃ and gray (19308) 1996 TO₆₆ TNOs were

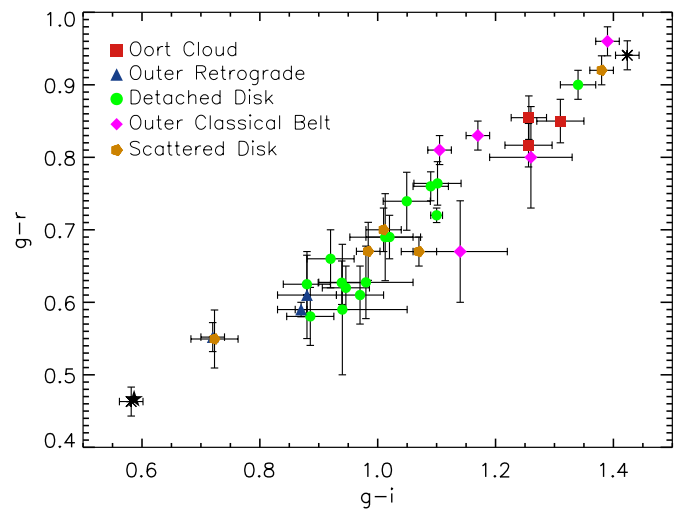


Figure 4. Same as Figure 2 except for Sloan colors $g' - i'$ and $g' - r'$. Colors with $g' - i' \gtrsim 1.2$, $g' - r' \gtrsim 0.8$, or $r' - i' \gtrsim 0.4$ mag indicate ultra-red colors (based on including the reddest 90% of the low inclination classical KBOs).

(A color version of this figure is available in the online journal.)

observed (Tegler & Romanishin 1998, 2000; Jewitt & Luu 2001; Barucci et al. 2005a). The $BVRI$ photometric results are shown in Table 2 (Figures 2 and 3) and the Sloan results in Table 3 (Figure 4).

Photometry was performed by optimizing the signal-to-noise ratio of the faint small outer solar system objects. Aperture correction photometry was done by using a small aperture on the TNOs ($0''.57$ – $0''.95$ in radius) and both the same small aperture and a large aperture ($2''.46$ – $3''.40$ in radius) on several nearby unsaturated bright field stars with similar point-spread functions (PSFs). The magnitude within the small aperture used for the TNOs was corrected by determining the correction from the small to the large aperture using the PSF of the field stars (cf. Tegler & Romanishin 2000; Jewitt & Luu 2001). For a few of the brighter objects (Sedna, 2003 FY₁₂₈, 2007 JJ₄₃, 2008 YB₃), both small apertures and the full large apertures were used on the TNOs to confirm both techniques obtained similar results.

3. RESULTS

The orbital parameters of the 33 outer solar system objects observed in this work are shown in Table 4. There were three main classes of objects in the observation sample: (1) objects dynamically linked to the inner Oort Cloud, (2) outer solar system retrograde and high inclination objects, and (3) extended or detached disk and outer classical belt objects. Each class is discussed in the subsections below. In addition, the well-measured gray object (19308) 1996 TO₆₆ that is part of the Haumea KBO collisional family and ultra-red object (44594) 1999 OX₃ were observed to confirm the photometry is consistent with previous works.

As seen in Figure 2, all objects observed appear to have correlated broadband optical colors. In other words, the objects appear to follow a nearly linear red slope in the optical. This has also been confirmed through spectroscopy and correlation analysis on other TNOs (Doressoundiram et al. 2008). Because of the near linearity in the optical colors, we can obtain the spectral gradient, S , of the objects using two unique optical broadband filters. The spectral gradient is basically a very low resolution spectrum of an object and is usually expressed in percent of reddening per 100 nm in wavelength. We follow

Table 1
Geometrical Circumstances of the Observations

Name	UT Date	R (AU)	Δ (AU)	α (deg)
(90377) Sedna	2008 Dec 3.267–.291	87.95	87.05	0.25
(48639) 1995 TL ₈	2009 Aug 25.289–.347	43.86	43.52	1.25
	2009 Aug 26.359–.373	43.86	43.50	1.24
(19308) 1996 TO ₆₆	2005 Nov 2.017–.028	46.47	45.64	0.67
(181874) 1999 HW ₁₁	2008 May 7.234–.299	42.99	42.00	0.26
(44594) 1999 OX ₃	2005 Nov 3.021–.033	24.48	24.36	2.31
(148209) 2000 CR ₁₀₅	2008 May 6.989–.999	56.57	56.46	1.02
	2008 May 7.000–.066	56.57	56.46	1.02
	2008 May 7.972–.999	56.57	56.48	1.02
	2008 May 8.000–.060	56.57	56.48	1.02
	2009 May 22.963–.999	57.08	57.22	1.01
	2009 May 23.000–.013	57.08	57.22	1.01
(118702) 2000 OM ₆₇	2009 Aug 25.201–.260	42.30	41.36	0.50
	2009 Aug 26.178–.231	42.30	41.36	0.48
(87269) 2000 OO ₆₇	2008 Oct 19.043–.065	21.30	20.38	1.01
2000 PE ₃₀	2008 May 7.390–.404	38.31	38.33	1.51
	2008 May 8.372–.389	38.32	38.31	1.51
(82075) 2000 YW ₁₃₄	2008 May 6.972–.989	43.86	44.04	1.29
	2008 May 7.963–.972	43.86	44.06	1.29
(182397) 2001 QW ₂₉₇	2008 May 7.366–.389	47.72	48.02	1.15
	2008 May 8.357–.372	47.72	48.00	1.16
	2008 May 8.390–.404	47.72	48.00	1.16
2002 GB ₃₂	2009 May 23.131–.165	35.65	34.88	1.07
	2009 May 24.087–.122	35.65	34.89	1.09
(84522) 2002 TC ₃₀₂	2009 Aug 26.278–.306	46.59	46.13	1.11
(127546) 2002 XU ₉₃	2009 Oct 15.596–.635	21.02	20.84	2.68
(120132) 2003 FY ₁₂₈	2008 May 7.214–.233	38.46	37.65	0.90
2003 FZ ₁₂₉	2008 May 7.106–.174	38.19	37.29	0.70
	2008 May 8.115–.135	38.19	37.30	0.72
2003 HB ₅₇	2009 May 24.122–.156	38.10	37.26	0.87
2003 QK ₉₁	2008 May 7.315–.365	39.63	39.69	1.46
	2008 May 8.339–.357	39.63	39.68	1.46
2003 UY ₂₉₁	2008 Dec 3.154–.228	43.29	42.32	0.19
	2009 Jan 28.000–.104	43.31	42.90	1.19
	2009 Aug 25.383–.421	43.38	43.41	1.33
2004 OJ ₁₄	2009 Aug 25.142–.200	45.39	44.54	0.69
	2009 Aug 26.144–.178	45.40	44.55	0.70
2004 VN ₁₁₂	2008 Oct 19.087–.105	47.33	46.37	0.35
	2008 Dec 3.052–.083	47.33	46.56	0.75
2004 XR ₁₉₀	2008 Dec 3.238–.267	58.08	57.10	0.05
2005 EO ₂₉₇	2008 May 7.070–.104	41.71	41.47	1.35
	2008 May 8.062–.115	41.71	41.49	1.35
2005 PU ₂₁	2009 Aug 26.101–.143	42.84	41.87	0.37
2005 SD ₂₇₈	2009 Aug 25.354–.383	41.75	41.53	1.36
	2009 Aug 26.373–.390	41.75	41.51	1.35
(145480) 2005 TB ₁₉₀	2008 May 7.405–.417	46.47	46.91	1.11
	2008 May 8.405–.419	46.47	46.89	1.12
2006 SQ ₃₇₂	2008 Oct 19.000–.038	41.81	42.64	0.75
2007 JJ ₄₃	2008 May 7.176–.212	41.86	40.87	0.34
2007 TG ₄₂₂	2008 Dec 3.229–.238	35.71	34.85	0.79
2007 VJ ₃₀₅	2009 Aug 25.261–.288	35.36	34.59	1.07
	2009 Aug 26.232–.270	35.36	34.58	1.05
2008 KV ₄₂	2009 May 23.166–.286	31.30	30.56	1.29
	2009 May 24.168–.224	31.29	30.56	1.29
2008 OG ₁₉	2009 Aug 25.083–.142	38.68	37.86	0.87
	2009 Aug 26.085–.101	38.68	37.87	0.89
2008 YB ₃	2009 May 23.013–.042	7.09	7.15	8.14

Notes. Quantities are the heliocentric distance (R), geocentric distance (Δ), and phase angle (α). UT date shows the year, month, day, and time span of the observations.

Doressoundiram et al. (2008) and express the spectral gradient as $S(\lambda_2 > \lambda_1) = (F_{2,V} - F_{1,V})/(\lambda_2 - \lambda_1)$, where λ_1 and λ_2 are the central wavelengths of the two filters used for the

calculation and $F_{1,V}$ and $F_{2,V}$ are the fluxes of the object in the two filters normalized to the V -band filter. S is the measure of the reddening of an object's surface determined between two

Table 2
BVRI Optical Photometry

Name (mag)	m_R (mag)	$m_R(1, 1, 0)$ (mag)	$m_B - m_R$ (mag)	$m_V - m_R$ (mag)	$m_R - m_I$ (mag)	$m_B - m_I$ (mag)
(90377) Sedna	20.49 ± 0.03	1.03 ± 0.05	1.68 ± 0.03	0.61 ± 0.03	0.66 ± 0.03	2.34 ± 0.04
(48639) 1995 TL ₈	21.04 ± 0.01	4.43 ± 0.03	1.86 ± 0.02	0.68 ± 0.02	0.64 ± 0.02	2.49 ± 0.02
(19308) 1996 TO ₆₆	21.10 ± 0.01	4.36 ± 0.02	1.06 ± 0.02	0.38 ± 0.02	0.33 ± 0.02	1.38 ± 0.02
(181874) 1999 HW ₁₁	22.93 ± 0.03	6.60 ± 0.05	1.32 ± 0.03	0.48 ± 0.03	0.52 ± 0.03	1.84 ± 0.04
(44594) 1999 OX ₃	20.98 ± 0.01	6.73 ± 0.02	1.82 ± 0.02	0.67 ± 0.02	0.69 ± 0.02	2.52 ± 0.02
(148209) 2000 CR ₁₀₅	23.84 ± 0.04	6.15 ± 0.07	1.26 ± 0.09	0.46 ± 0.09	0.59 ± 0.09	1.85 ± 0.11
(118702) 2000 OM ₆₇	23.29 ± 0.03	7.00 ± 0.05	1.29 ± 0.04	0.47 ± 0.04	0.59 ± 0.04	1.88 ± 0.04
(87269) 2000 OO ₆₇	22.11 ± 0.02	8.76 ± 0.04	1.69 ± 0.03	0.61 ± 0.03	0.61 ± 0.03	2.30 ± 0.03
2000 PE ₃₀	21.61 ± 0.02	5.53 ± 0.03	1.19 ± 0.04	0.43 ± 0.04	0.38 ± 0.03	1.58 ± 0.04
(82075) 2000 YW ₁₃₄	20.86 ± 0.03	4.22 ± 0.05	1.50 ± 0.04	0.55 ± 0.04	0.55 ± 0.03	2.05 ± 0.04
(182397) 2001 QW ₂₉₇	23.46 ± 0.05	6.47 ± 0.08	1.60 ± 0.07	0.58 ± 0.07	0.67 ± 0.06	2.27 ± 0.07
2002 GB ₃₂	23.11 ± 0.01	7.47 ± 0.03	1.39 ± 0.02	0.51 ± 0.02	0.61 ± 0.02	2.00 ± 0.03
(84522) 2002 TC ₃₀₂	20.38 ± 0.02	3.54 ± 0.04	1.76 ± 0.02	0.64 ± 0.02	0.66 ± 0.02	2.42 ± 0.03
(127546) 2002 XU ₉₃	21.15 ± 0.01	7.52 ± 0.03	1.20 ± 0.02	0.44 ± 0.02	0.38 ± 0.02	1.58 ± 0.02
(120132) 2003 FY ₁₂₈	20.28 ± 0.01	4.34 ± 0.02	1.65 ± 0.02	0.60 ± 0.02	0.55 ± 0.03	2.20 ± 0.03
2003 FZ ₁₂₉	22.75 ± 0.02	6.87 ± 0.04	1.32 ± 0.04	0.48 ± 0.04	0.46 ± 0.03	1.78 ± 0.04
2003 HB ₅₇	23.15 ± 0.02	7.25 ± 0.02	1.31 ± 0.03	0.48 ± 0.03	0.54 ± 0.03	1.84 ± 0.04
2003 QK ₉₁	22.95 ± 0.03	6.73 ± 0.05	1.37 ± 0.04	0.50 ± 0.04	0.47 ± 0.03	1.84 ± 0.04
2003 UY ₂₉₁	23.36 ± 0.05 ^a	5.78 ± 0.08	1.39 ± 0.07	0.51 ± 0.07	0.67 ± 0.07	2.06 ± 0.08
2004 OJ ₁₄	23.52 ± 0.02	6.88 ± 0.04	1.42 ± 0.03	0.52 ± 0.03	0.54 ± 0.03	1.96 ± 0.04
2004 VN ₁₁₂	22.82 ± 0.04	5.98 ± 0.06	1.42 ± 0.06	0.52 ± 0.06	0.45 ± 0.06	1.87 ± 0.06
2004 XR ₁₉₀	21.54 ± 0.03	3.93 ± 0.05	1.24 ± 0.04	0.45 ± 0.04	0.52 ± 0.04	1.76 ± 0.04
2005 EO ₂₉₇	23.41 ± 0.03 ^a	7.00 ± 0.06	1.32 ± 0.05	0.48 ± 0.05	0.57 ± 0.08	1.89 ± 0.08
2005 PU ₂₁	22.36 ± 0.02	6.03 ± 0.04	1.79 ± 0.02	0.65 ± 0.02	0.68 ± 0.02	2.47 ± 0.02
2005 SD ₂₇₈	22.11 ± 0.02	5.70 ± 0.04	1.53 ± 0.02	0.56 ± 0.02	0.53 ± 0.02	2.06 ± 0.03
(145480) 2005 TB ₁₉₀	20.86 ± 0.02	3.99 ± 0.04	1.54 ± 0.03	0.56 ± 0.03	0.55 ± 0.03	2.09 ± 0.04
2006 SQ ₃₇₂	21.48 ± 0.02	5.11 ± 0.04	1.62 ± 0.03	0.59 ± 0.03	0.65 ± 0.04	2.27 ± 0.04
2007 JJ ₄₃	20.21 ± 0.01	3.99 ± 0.02	1.61 ± 0.02	0.59 ± 0.02	0.50 ± 0.02	2.12 ± 0.02
2007 TG ₄₂₂	21.66 ± 0.01	6.05 ± 0.03	1.39 ± 0.04	0.51 ± 0.04	0.51 ± 0.04	1.90 ± 0.02
2007 VJ ₃₀₅	22.15 ± 0.02	6.54 ± 0.04	1.44 ± 0.03	0.52 ± 0.03	0.52 ± 0.03	1.96 ± 0.03
2008 KV ₄₂	23.47 ± 0.04 ^a	8.36 ± 0.07	1.29 ± 0.06	0.47 ± 0.06	0.42 ± 0.06	1.71 ± 0.06
2008 OG ₁₉	20.44 ± 0.01	4.47 ± 0.02	1.47 ± 0.01	0.53 ± 0.01	0.59 ± 0.01	2.06 ± 0.01
2008 YB ₃	18.24 ± 0.01	8.41 ± 0.02	1.26 ± 0.01	0.46 ± 0.01	0.49 ± 0.01	1.75 ± 0.01

Notes. A few of the above objects have also had colors independently determined. In most cases, the colors reported elsewhere and found in this work are within the uncertainties of the various observations. 1995 TL₈ has large uncertainties from *BVRI* data of Doressoundiram et al. (2002) and Delsanti et al. (2001); our results agree with Delsanti et al. (2001) and are inconsistent with Doressoundiram et al. (2002); 1999 HW₁₁ has *BVR* data from Trujillo & Brown (2002); 2000 PE₃₀ has *BVRI* data from Doressoundiram et al. (2001); 2000 YW₁₃₄ has *BVRI* data from Tegler & Romanishin (2003), Peixinho et al. (2004), Doressoundiram et al. (2007), Jewitt et al. (2007), and Santos-Sanz et al. (2009); 2000 CR₁₀₅ has *BVR* data from Tegler & Romanishin (2003) and *VRI* data from Santos-Sanz et al. (2009); 2000 OO₆₇ has *BVR* data with large uncertainties from Tegler & Romanishin (2003); 2003 FY₁₂₈ has *VRI* data from DeMeo et al. (2009).

^a These few objects showed large light variations during the observations indicating possible significant rotational light curves (>0.1 mag). Their colors were consistent throughout the observations since the variations caused by possible light curves were similar in all filters. Filters were also rotated after each observation to prevent a light curve from influencing the color calculation. The apparent magnitude (m_R) and calculated absolute magnitude ($m_R(1, 1, 0)$) are based on the average of the photometry.

wavelength measurements (two different filters). We determined the spectral gradient of the observed objects using the g' and i' filters, which have well-separated central wavelengths of 481.3 and 773.2 nm, respectively. The spectral gradient results for the observed objects are shown in Table 3, and the spectral gradient determined for known small body populations in the solar system are shown in Table 5. Ultra-red color is here defined as including the reddest 90% of the measured low inclination classical KBOs (ultra-red: $S \gtrsim 25$, $B-R \gtrsim 1.6$, $V-I \gtrsim 1.2$, $B-I \gtrsim 2.2$, $V-R \gtrsim 0.6$, $R-I \gtrsim 0.6$, and using Sloan colors $g' - i' \gtrsim 1.2$, $g' - r' \gtrsim 0.8$, and $r' - i' \gtrsim 0.4$ mag).

3.1. Inner Oort Cloud Objects

The Oort Cloud is believed to have formed from the scattering of planetismals from the giant planet region during early planet

formation and is usually separated into two parts (Oort 1950; Stern 2003; Leto et al. 2008; Brassier 2008). The inner Oort Cloud is within a few thousands to ten thousand AU and is fairly stable to Galactic tides and passing star perturbations unlike the outer Oort Cloud at several tens of thousands of AU. While the short-period comets are all likely from the Kuiper Belt region's scattered disk population (Duncan et al. 2004; Levison et al. 2006), the long-period comets are believed to be from the Oort Cloud (Kaib & Quinn 2009). All the known long-period comets have perihelia within about 10 AU of the Sun. The surfaces of the long-period comets have already been highly altered before they are first observed because of the thermal and sublimation processes that occur as they approach the Sun (Meech et al. 2009).

Sedna was the first object suggested to be part of the inner Oort Cloud (Brown et al. 2004). Recently, Kaib et al. (2009)

Table 3
Sloan g' , r' , i' Optical Photometry

Name	$m_{r'}$ (mag)	S^a	$g' - r'$ (mag)	$r' - i'$ (mag)	$g' - i'$ (mag)
(90377) Sedna	20.75 ± 0.03	26.3 ± 3	0.85 ± 0.03	0.45 ± 0.03	1.31 ± 0.04
(48639) 1995 TL ₈	21.31 ± 0.01 ^b	29.4 ± 2	0.96 ± 0.02	0.43 ± 0.02	1.39 ± 0.02
(19308) 1996 TO ₆₆	21.31 ± 0.01	-0.15 ± 1	0.46 ± 0.02	0.12 ± 0.02	0.58 ± 0.02
(181874) 1999 HW ₁₁	23.15 ± 0.03	12.2 ± 3	0.63 ± 0.03	0.31 ± 0.03	0.94 ± 0.04
(44594) 1999 OX ₃	21.25 ± 0.01	31.5 ± 2	0.94 ± 0.02	0.48 ± 0.02	1.42 ± 0.02
(148209) 2000 CR ₁₀₅	24.06 ± 0.04	13.7 ± 6	0.59 ± 0.09	0.38 ± 0.09	0.94 ± 0.11
(118702) 2000 OM ₆₇	23.52 ± 0.03	14.4 ± 3	0.61 ± 0.04	0.38 ± 0.04	0.97 ± 0.04
(87269) 2000 OO ₆₇	22.37 ± 0.02	24.1 ± 3	0.85 ± 0.03	0.40 ± 0.03	1.26 ± 0.03
2000 PE ₃₀	21.83 ± 0.02	4.4 ± 3	0.55 ± 0.04	0.17 ± 0.03	0.72 ± 0.04
(82075) 2000 YW ₁₃₄	21.10 ± 0.03	17.1 ± 3	0.74 ± 0.04	0.34 ± 0.03	1.05 ± 0.04
(182397) 2001 QW ₂₉₇	23.71 ± 0.05	25.0 ± 5	0.80 ± 0.07	0.46 ± 0.06	1.26 ± 0.07
2002 GB ₃₂	23.35 ± 0.01	17.4 ± 3	0.67 ± 0.02	0.40 ± 0.02	1.07 ± 0.03
(84522) 2002 TC ₃₀₂	20.65 ± 0.02	28.2 ± 3	0.90 ± 0.02	0.45 ± 0.02	1.34 ± 0.03
(127546) 2002 XU ₉₃	21.37 ± 0.01	4.4 ± 2	0.55 ± 0.02	0.17 ± 0.02	0.72 ± 0.02
(120132) 2003 FY ₁₂₈	20.54 ± 0.01	20.4 ± 3	0.83 ± 0.02	0.34 ± 0.02	1.17 ± 0.02
2003 FZ ₁₂₉	22.98 ± 0.02	9.9 ± 3	0.62 ± 0.04	0.25 ± 0.03	0.88 ± 0.04
2003 HB ₅₇	23.38 ± 0.02	12.5 ± 3	0.62 ± 0.03	0.33 ± 0.03	0.95 ± 0.04
2003 QK ₉₁	23.18 ± 0.03	11.2 ± 3	0.66 ± 0.04	0.26 ± 0.03	0.92 ± 0.04
2003 UY ₂₉₁	23.59 ± 0.05 ^b	19.9 ± 7	0.67 ± 0.07	0.46 ± 0.07	1.14 ± 0.08
2004 OJ ₁₄	23.76 ± 0.02	15.1 ± 3	0.69 ± 0.03	0.33 ± 0.03	1.02 ± 0.04
2004 VN ₁₁₂	23.06 ± 0.04	11.3 ± 4	0.69 ± 0.06	0.24 ± 0.06	1.01 ± 0.06
2004 XR ₁₉₀	21.76 ± 0.03	10.3 ± 3	0.58 ± 0.04	0.31 ± 0.04	0.89 ± 0.04
2005 EO ₂₉₇	23.64 ± 0.03 ^b	14.0 ± 6	0.63 ± 0.05	0.36 ± 0.08	0.98 ± 0.08
2005 PU ₂₁	22.63 ± 0.02	30.0 ± 3	0.92 ± 0.02	0.47 ± 0.02	1.38 ± 0.02
2005 SD ₂₇₈	22.36 ± 0.02	17.1 ± 3	0.76 ± 0.02	0.32 ± 0.02	1.09 ± 0.03
(145480) 2005 TB ₁₉₀	21.11 ± 0.02	18.1 ± 3	0.76 ± 0.03	0.34 ± 0.03	1.10 ± 0.04
2006 SQ ₃₇₂	21.74 ± 0.02	24.6 ± 3	0.82 ± 0.03	0.44 ± 0.04	1.26 ± 0.04
2007 JJ ₄₃	20.46 ± 0.01	17.7 ± 3	0.81 ± 0.02	0.29 ± 0.02	1.11 ± 0.02
2007 TG ₄₂₂	21.89 ± 0.01	13.3 ± 1	0.67 ± 0.04	0.30 ± 0.04	0.98 ± 0.02
2007 VJ ₃₀₅	22.39 ± 0.02	14.6 ± 3	0.70 ± 0.03	0.31 ± 0.03	1.01 ± 0.03
2008 KV ₄₂	23.70 ± 0.04 ^b	7.7 ± 4	0.61 ± 0.06	0.21 ± 0.06	0.88 ± 0.06
2008 OG ₁₉	20.68 ± 0.01 ^b	18.3 ± 2	0.72 ± 0.01	0.38 ± 0.01	1.10 ± 0.01
2008 YB ₃	18.46 ± 0.01	9.6 ± 0.5	0.59 ± 0.01	0.28 ± 0.01	0.87 ± 0.01

Notes.

^a The normalized spectral gradient for the optical colors of the observed objects (see the text for details).

^b These few objects showed large light variations during the observations indicating possible significant rotational light curves (> 0.1 mag). Their colors were consistent throughout the observations since the variations caused by possible light curves were similar in all filters. Filters were rotated during the observations in order to prevent any rotational light curve from influencing the color results. The apparent magnitude is based on the average of the photometry.

have suggested through dynamical simulations that the relatively large perihelia and semimajor axes of 2006 SQ₃₇₂ and (87269) 2000 OO₆₇ also make them likely objects from the inner Oort Cloud. The three inner Oort Cloud objects Sedna, 2006 SQ₃₇₂, and 2000 OO₆₇ could be the first objects from the inner Oort Cloud region that we have observed with thermally unaltered surfaces. These inner Oort Cloud objects are likely to have formed in a different location than many of the KBOs.

The observations obtained of these three possible inner Oort Cloud objects in this work show all to be among the reddest objects observed in this sample. Their surfaces are of ultra-red material ($S \gtrsim 25$). Though all three having ultra-red material are a promising trend, more inner Oort Cloud type objects are needed to be discovered (see Schwamb et al. 2009) in order to confirm a strong significant (3σ) color correlation for inner Oort Cloud objects and ultra-red material. The spectral gradients of the possible inner Oort Cloud objects are very similar to the red lobe of the Centaur distribution, the low inclination classical KBOs, and outer classical belt KBOs (Table 5). As discussed in the introduction, ultra-red material is likely rich in organic material (Barucci et al. 2008).

3.2. Retrograde and High Inclination Objects

Until recently all known retrograde objects had perihelia within the inner solar system. In the last year, two objects have been discovered with retrograde orbits and perihelia in the giant planet region. Neither shows any current evidence of cometary activity. 2008 YB₃ has a perihelion around 6.5 AU and thus is likely to have undergone surface sublimation and interior recrystallization during its lifetime (Meech et al. 2009). 2008 KV₄₂ has a perihelion of about 21 AU and thus the amount of surface alteration of this object could be significantly less than other retrograde objects and comet-type objects. Gladman et al. (2009) simulated the orbit of 2008 KV₄₂ and found its perihelion distance likely has not been interior to Saturn over the age of the solar system. It is unknown where 2008 KV₄₂ came from but its orbit is similar to Halley's comet, and thus it could have come from the Oort Cloud or another yet to be discovered high inclination reservoir.

The observations obtained of these two outer solar system retrograde objects and the similar high inclination object (127546) 2002 XU₉₃ show all to have only moderately red surfaces

Table 4
Orbital Information for Observed Objects

Name	Type ^a	q (AU)	a (AU)	e	i (deg)
(90377) Sedna	Oort(3),Det(1,9)	76.3	501	0.85	11.9
(48639) 1995 TL ₈	Det(9),Obelt(1)	40.0	52.6	0.24	0.2
(19308) 1996 TO ₆₆	Fam(4)	38.3	43.4	0.12	27.4
(181874) 1999 HW ₁₁	Det(1,2)	39.2	52.7	0.26	17.2
(44594) 1999 OX ₃	Sca(1)	17.6	32.5	0.46	2.6
(148209) 2000 CR ₁₀₅	Det(1,2,9)	44.1	218	0.80	22.8
(118702) 2000 OM ₆₇	Det(1)	39.2	100.0	0.61	23.3
(87269) 2000 OO ₆₇	Oort(5),Sca(1)	20.8	639	0.97	20.1
2000 PE ₃₀	Det(1)	35.8	54.9	0.35	18.4
(82075) 2000 YW ₁₃₄	Det(9),Res(1)	41.1	57.6	0.29	19.9
(182397) 2001 QW ₂₉₇	Det(2),Obelt(1)	39.7	52.0	0.24	17.0
2002 GB ₃₂	Sca(1,2)	35.3	208	0.83	14.2
(84522) 2002 TC ₃₀₂	Det,Res(1)	39.2	55.3	0.29	35.0
(127546) 2002 XU ₉₃	High Incl(6)	21.0	66.5	0.68	78.0
(120132) 2003 FY ₁₂₈	Det(1),Obelt	37.1	49.3	0.25	11.8
2003 FZ ₁₂₉	Det(1,9)	38.0	61.7	0.38	5.8
2003 HB ₅₇	Sca(1)	38.1	160	0.76	15.5
2003 QK ₉₁	Det(1,9)	38.5	68.5	0.44	4.0
2003 UY ₂₉₁	Det(2,9),Obelt(1)	41.2	49.2	0.16	3.5
2004 OJ ₁₄	Det	39.4	55.7	0.29	22.4
2004 VN ₁₁₂	Det(7)	47.3	337	0.86	25.6
2004 XR ₁₉₀	Det(8,9),Obelt(1)	51.3	57.4	0.11	46.7
2005 EO ₂₉₇	Det	41.1	62.4	0.34	25.1
2005 PU ₂₁	Sca	29.4	178	0.835	6.2
2005 SD ₂₇₈	Det	39.8	55.6	0.284	17.8
(145480) 2005 TB ₁₉₀	Det(9)	46.2	76.5	0.40	26.4
2006 SQ ₃₇₂	Oort(5)	24.2	1082	0.98	19.5
2007 JJ ₄₃	Det,Obelt	40.2	48.3	0.17	12.0
2007 TG ₄₂₂	Sca	35.5	528	0.93	18.6
2007 VJ ₃₀₅	Sca	35.2	199	0.823	12.0
2008 KV ₄₂	Retro(6)	21.2	41.8	0.49	103.4
2008 OG ₁₉	Det	38.6	67.4	0.428	13.1
2008 YB ₃	Retro	6.5	11.6	0.44	105.1

Notes. Quantities are the perihelion distance (q), semimajor axis (a), eccentricity (e), and inclination (i). Data taken from the Minor Planet Center.

^a Det: detached disk; Fam: (136108) Haumea (2003 EL₆₁) collisional family member; High Incl: high inclination object; Obelt: outer classical belt; Oort: inner Oort cloud; Res: resonance object; Retro: retrograde outer solar system object; Sca: scattered disk.

References. (1) Gladman et al. 2008; (2) Elliot et al. 2005; (3) Brown et al. 2004; (4) Ragozzine & Brown 2007; (5) Kaib et al. 2009; (6) Gladman et al. 2009; (7) Becker et al. 2008; (8) Allen et al. 2006; (9) Lykawka & Mukai 2007a.

($S \sim 9$). Their spectral gradients are similar to the known comets, extinct comet objects, Jupiter Trojans, Neptune Trojans, irregular satellites, and damocloids (Table 5). This suggests the outer retrograde and high inclination object surfaces have been thermally altered over the age of the solar system as is expected for these other similarly moderately red colored volatile-rich objects.

3.3. Extended/Detached Disk and Outer Classical Belt Objects

Objects with large semimajor axes and perihelion distances have only recently been discovered (Gladman et al. 2002). Knowledge of the physical properties of these dynamically interesting objects is important to constrain their origins and evolution. Detached disk objects are considered to have moderate to large eccentricities ($e > 0.2-0.25$), large perihelion distances ($q \gtrsim 38$ AU), and large semimajor axes ($50 \lesssim a \lesssim 500$ AU; Elliot et al. 2005; Lykawka & Mukai 2007a; Gladman et al. 2008). Detached disk objects are somewhat decoupled from

Table 5
Spectral Gradients of Small Solar System Objects

Name	S^a	Reference
==== Neutral color =====	====	==
Haumea KBO family	0.7 ± 2	1,9,13
C-type asteroids	2.0 ± 2	20
====Moderate red color=====	====	==
Dead comets	7.2 ± 5	2
Jupiter Trojans	7.6 ± 3	6,18,19,20
Irregular satellites	7.8 ± 5	7,10,11
Neutral Centaur lobe	8.2 ± 5	8,15,17,21
Outer retrograde	8.7 ± 2	1
D-type asteroids	8.9 ± 3	5,20
Neptune Trojans	9.1 ± 3	4
Comets	10.0 ± 3	2,14,22
==== Red color =====	====	==
Scattered KBOs	10.1 ± 5	1,8,12
Damocloids	11.9 ± 3	3
Detached disk	14.5 ± 5	1
Plutinos	16.9 ± 5	8,12
High Incl. classical	19.9 ± 10	8,12
All Centaurs	20.5 ± 15	8,12,15,21
All KBOs	20.7 ± 15	8,12,15
All cubewanos	22.4 ± 15	8,12,15
==== Very red color =====	====	==
Outer classical belt	22.8 ± 5	1
High-order resonance	23.7 ± 10	1,8,12
==== Ultra-red color =====	====	==
Inner Oort cloud	25.0 ± 2	1
Low Incl. classical	27.4 ± 5	8,12,16
Red Centaur lobe	34.3 ± 5	8,15,17,21

Notes.

^a Spectral gradient as defined in the text using known B - or g' - and I - or i' -band photometry normalized to the V band. The \pm on the spectral gradient is not an error but displays the general range the type of objects span.

References. (1) This work; (2) Jewitt 2002; (3) Jewitt 2005; (4) Sheppard & Trujillo 2006; (5) Fitzsimmons et al. 1994; (6) Fornasier et al. 2007; (7) Grav et al. 2003; (8) Barucci et al. 2005a; (9) Tegler & Romanishin 2003; (10) Grav et al. 2004; (11) Grav & Bauer 2007; (12) Hainaut & Delsanti 2002 (including updated MBOSS Web site); (13) Ragozzine & Brown 2007; (14) Lamy & Toth 2009; (15) Peixinho et al. 2004; (16) Peixinho et al. 2008; (17) Peixinho et al. 2003; (18) Karlsson et al. 2009; (19) Melita et al. 2008; (20) Roig et al. 2008; (21) Bauer et al. 2003; (22) Snodgrass et al. 2008.

the giant planet region yet have been considerably influenced dynamically to obtain their relatively large eccentricities. The objects in the detached disk can thus be considered intermediate between the Kuiper Belt and the inner Oort Cloud. Objects with dynamics closely related to the detached disk are the outer classical belt population. The outer classical belt objects have $a > 48.4$ AU, $e < 0.25$ and are nonresonant (Gladman et al. 2008). Objects with $39.4 < a < 48.4$ AU and $e < 0.25$ are considered main classical belt objects or cubewanos. The 2:1 Neptune resonance separates the main classical belt from the outer classical belt.

In this work, most of the known detached disk and outer classical belt objects were observed to determine their optical colors for the first time in order to compare them to other solar system small body reservoirs. In particular, determining if these populations are dominated by ultra-red material allows important constraints to be placed on the origin and evolution of these populations.

3.3.1. Detached Disk

Though the detached disk has been defined differently by various authors, this work takes a very strict definition. A detached disk object must have $q > 38$ AU, $e > 0.25$, and $50 < a < 500$ AU. Thus 13 objects that were observed in this work qualify as detached disk objects under this definition (2008 OG₁₉, 2005 SD₂₇₈, (145480) 2005 TB₁₉₀, 2004 OJ₁₄, 2004 VN₁₁₂, 2003 QK₉₁, 2005 EO₂₉₇, 2003 FZ₁₂₉, (84522) 2002 TC₃₀₂, (148209) 2000 CR₁₀₅, (82075) 2000 YW₁₃₄, (118702) 2000 OM₆₇, (181874) 1999 HW₁₁).

The colors of the detached disk objects do not appear to be extraordinary (Figure 2). Except for one ultra-red detached disk object, the rest show only moderately red colors ($10 \lesssim S \lesssim 18$). Their spectral gradient average ($S = 14.5 \pm 5$) is very similar to the scattered disk KBOs, Plutinos, high inclination classical KBOs as well as the damocloids and comets (Table 5). The detached disk objects are thus not likely from the same source region as the ultra-red low inclination classical KBO population or the inner Oort Cloud though if they are from the same source region than the detached disk objects had significantly different surface altering histories. Inclination is not important in the color of detached disk objects with even the few very low inclination objects observed in the detached disk (2003 FZ₁₂₉ and 2003 QK₉₁) showing only moderately red colors. The discovery of more low inclination detached disk objects is needed to further confirm that this population is not rich in ultra-red material unlike the low inclination main classical belt. The only detached disk object found to have ultra-red surface material is (84522) 2002 TC₃₀₂, which has a large inclination of 35° . (84522) 2002 TC₃₀₂ is possibly in the 5:2 Neptune resonance and as discussed below it appears objects in high-order Neptune resonances are on average very red.

3.3.2. Outer Classical Belt Objects

The outer classical belt objects have $a > 48.4$ AU, $e < 0.25$, $i < 40^\circ$ and are nonresonant. Outer classical belt objects are separated from the main classical belt by the 2:1 resonance and have slightly smaller eccentricities than the detached disk objects. The observed sample has five bona fide outer classical belt objects (2007 JJ₄₃, (120132) 2003 FY₁₂₈, 2003 UY₂₉₁, (182397) 2001 QW₂₉₇, and (48639) 1995 TL₈).

The only other possible outer disk object in our sample would be 2004 XR₁₉₀. This is a very dynamically unusual object since it has a relatively low eccentricity, large semimajor axis, and large inclination (Table 4). It is to date a dynamically unique object but has been classified as an outer disk object by Gladman et al. (2008) and a detached disk object by Allen et al. (2006) and Lykawka & Mukai (2007a). Gomes et al. (2008) believe that 2004 XR₁₉₀ is a fossil-detached object. 2004 XR₁₉₀ was likely scattered by a close planetary encounter into the 3:8 mean motion resonance with Neptune. 2004 XR₁₉₀ then escaped from the 3:8 mean motion resonance while Neptune was still migrating outward during the very early evolution of the solar system. Scattering and escaping the mean motion resonance would help explain the rather large inclination, large perihelion distance, and large size of 2004 XR₁₉₀. In addition, the Gomes (2003) model found outer classical belt objects are not expected to obtain such high inclinations as 2004 XR₁₉₀. 2004 XR₁₉₀ has only a moderately red color of $S = 10.3 \pm 3$ like the higher eccentricity detached objects (further discussion of 2004 XR₁₉₀ is in Section 4).

Excluding the dynamically unique 2004 XR₁₉₀, the outer classical belt objects are significantly redder ($18 \lesssim S \lesssim 30$) than the average detached disk objects ($10 \lesssim S \lesssim 18$). The average outer classical belt objects spectral gradient ($S = 22.8 \pm 5$ or $S = 21.0 \pm 5$ if including 2004 XR₁₉₀) is similar to the ultra-red material seen in the low inclination classical Kuiper Belt and inner Oort Cloud objects (Table 5). The sample of outer classical belt objects are all very red even though they cover a wide range of inclinations with both 2003 UY₂₉₁ and 1995 TL₈ having very low inclinations ($i < 4^\circ$) and 2001 QW₂₉₇, 2003 FY₁₂₈ and 2007 JJ₄₃ having moderate inclinations ($i \sim 12^\circ - 17^\circ$). This is unlike the main classical belt where the low inclination objects are dominated by ultra-red objects ($S \gtrsim 25$) while the higher inclination objects are not dominated by ultra-red material. More outer classical belt objects need to be discovered to confirm this population is dominated by very red objects ($S \gtrsim 20$).

4. DISCUSSION

4.1. Detached and Scattered Disk

The scattered disk is probably made up of two main source populations. Some scattered disk objects are likely the surviving members of a relic population of objects that were scattered during Neptune's migration in the very early solar system (Gomes et al. 2008). A second source for the scattered disk is from recently dislodged objects from the Kuiper Belt through various slow dynamical processes (resonances) or collisions (Duncan et al. 1995; Levison & Duncan 1997; Duncan & Levison 1997; Nesvorný & Roig 2001; Gomes et al. 2008).

How the detached disk may have formed is still an open question (Gomes et al. 2008; Morbidelli et al. 2008; Kenyon et al. 2008; Duncan et al. 2008b; Gladman et al. 2008). For high inclination objects ($i > 50^\circ$) the Kozai resonance can allow scattered objects to obtain large perihelion distances (Thomas & Morbidelli 1996; Gallardo 2006). For objects with moderate inclinations, the Kozai mechanism only works in increasing the perihelion distance of a scattered object if the object is also in a mean motion resonance with Neptune (Gomes 2003). Using Neptune mean motion resonances and the Kozai mechanism, Gomes et al. (2008) believe the high perihelia and relatively large semimajor axes of some moderate inclination detached objects can be explained through the above mechanism, specifically 2000 YW₁₃₄, 2005 EO₂₉₇, and 2005 TB₁₉₀ as well as the high inclination object 2004 XR₁₉₀, since they are all in or near Neptune mean motion resonances. These objects were likely at some point scattered disk objects that simply had their perihelia raised through Neptune mean motion resonances and the Kozai effect.

Based on the similar average spectral gradients of the two populations, the origin of the objects in the detached disk could be similar as the scattered disk (Table 5). The scattered disk spectral gradient ($S = 10.1 \pm 5$) shown in Table 5 uses the strict definition similar to Gladman et al. (2008) which eliminates objects thought to be in any resonance with Neptune from being called a scattered disk object (called here the strict scattered disk: objects not in an obvious high-order resonance with Neptune, perihelia less than 35 AU, and semimajor axis between 30 and 100 AU). If objects in high-order resonances with Neptune are allowed in the definition used for what is a scattered disk object, the spectral gradient increases slightly and is almost the same as the detached disk average spectral gradient (14.5 ± 5). It is interesting to note that very red ($S \gtrsim 20$) objects are absent in the strict definition of the scattered disk but are not when

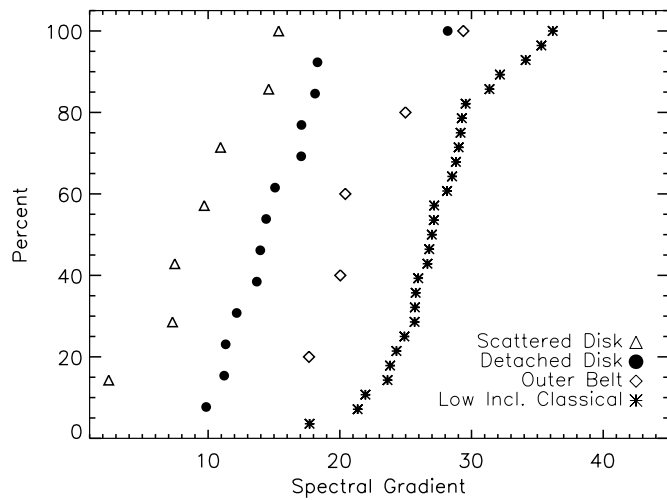


Figure 5. Kolmogorov–Smirnov test plotted for the detached disk (circles), outer classical belt (diamonds), low inclination “cold” classical belt (asterisks), and strict scattered disk objects (triangles: not including objects thought to be in high-order resonances with Neptune, having perihelia above 35 AU or semimajor axes above 100 AU). The vertical axis shows the cumulative spectral gradient for the objects. It is clear that the groups have some overlap in color but on average the low inclination classical belt objects are the reddest followed by the outer classical belt objects, the detached disk objects, and the most neutral objects being the scattered disk. The results of comparing various population spectral gradient distributions are shown in Table 6.

including the higher order resonance objects. This may hint that many high-order resonance scattered disk objects are coming from the ultra-red low inclination classical belt or outer classical belt objects. It may be that the only efficient way to dislodge these fairly dynamically stable ultra-red objects is through some resonance interactions.

To further compare the scattered disk to the detached disk population, the Student’s t -test and the Kolmogorov–Smirnov (K–S) test were performed on the spectral gradients of the two populations (Figure 5). The differences in the two population distributions were not statistically significant ($< 3\sigma$) in either test and thus are consistent with both populations coming from the same parent population (Table 6). This is true no matter if the high-order outer resonance objects are considered scattered disk objects or not (Figure 6). The similarity of spectral gradients may hint that Neptune mean motion and Kozai resonances allowed scattered disk objects to become detached overtime from significant Neptune influence and that the detached disk is a simple extension of the scattered disk (Gallardo 2006; Lykawka & Mukai 2007b; Emel’yanenko & Kiseleva 2008; Gladman et al. 2008; Gomes et al. 2008). Based on the spectral gradients and dynamics of the objects in the detached and scattered disk, it appears that they likely contain many objects from the same source region.

4.2. Ultra-red Colors and the Outer Classical Belt

The outer classical belt objects have lower eccentricities and usually lower semimajor axes than the detached disk objects. They are separated from the main classical belt by the Neptune 2:1 mean motion resonance. The dynamical origin of the outer classical belt objects are not easy to explain through simple Neptune mean motion resonances and the Kozai effect, and may have a different origin than the detached disk objects (Gomes 2003; Gomes et al. 2008; Morbidelli et al. 2008). Simulations by Gomes (2003) of Neptune’s migration and the formation of the Kuiper Belt show that the objects coming from the

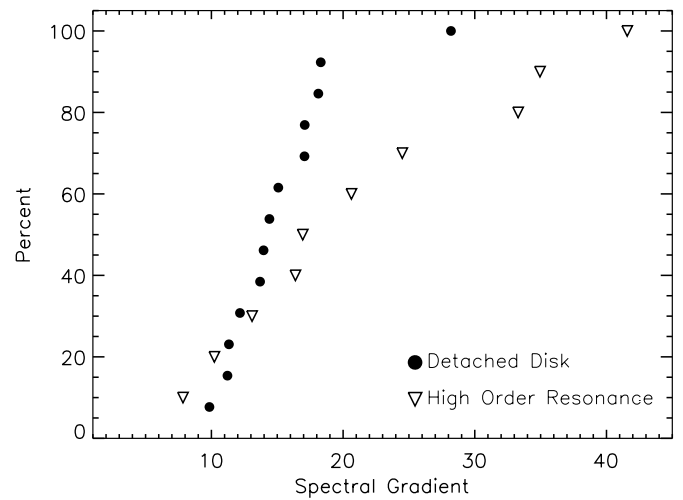


Figure 6. Same as Figure 5 except showing scattered disk objects thought to be in high-order resonances with Neptune (upside down triangles). The high-order resonance objects consist of a wide range of spectral gradients including a significant amount of ultra-red objects.

Table 6
t-test and Kolmogorov–Smirnov Test Results

Type 1 ^a	Type 2 ^a	N ^b	<i>t</i> -stat ^c	<i>t</i> -test ^d	D-stat ^e	K–S ^d
Detached disk	Cold classical	41	8.88	99.99%	0.88	99.99%
Scattered strict	Cold classical	35	10.49	99.98%	0.86	99.98%
3 σ		99.73%
High-order res.	Cold classical	38	2.48	83%	0.56	98.97%
Outer belt	Scattered strict	12	−3.76	99.88%	0.86	98.96%
Detached disk	Outer belt	18	3.87	97.7%	0.77	98.79%
Detached disk	Scattered strict	20	−1.68	98.1%	0.64	97.3%
2 σ		95%
Outer belt	Cold classical	33	3.20	92%	0.56	92%
High-order res.	Scattered strict	17	−2.08	99.09%	0.56	90%
Detached disk	High-order res.	23	2.70	88%	0.42	80%
Outer belt	High-order res.	15	1.13	10%	0.50	75%

Notes.

^a The dynamical groups being tested.

^b The number of objects used in the test.

^c The t -statistic from the t -test.

^d The level of confidence that the two groups are not drawn from the same parent population using the t -test or the K–S test.

^e The D-statistic from the K–S test.

outer most portion of the disk that Neptune migrates through would have preferentially low inclinations ($i < 10^\circ$) and low eccentricities ($e \lesssim 0.1$) when dispersed to near 40 AU. This is likely the source of the “cold” classical disk (see Gomes 2003; Figure 2). The inclination distribution for these objects is found in the simulations to increase slightly at larger semimajor axes. More importantly, the Gomes simulations show that these same objects further out in semimajor axis around 50 AU would have significantly larger eccentricities ($e \sim 0.2$). Using these ideas, Gomes et al. (2008) suggest that objects with orbits like the outer classical belt are not fossilized detached disk objects and more likely share a similar origin as the low inclination “cold” classical population (Gomes 2003; Morbidelli et al. 2008). The very red colors ($S \gtrsim 20$) found in this work for these outer classical belt objects support this hypothesis. The spectral gradient of the outer classical belt objects averages $S = 22.8 \pm 5$ which is similar to that found for the low inclination “cold” classical main belt objects (27.4 ± 5 ; see Table 5).

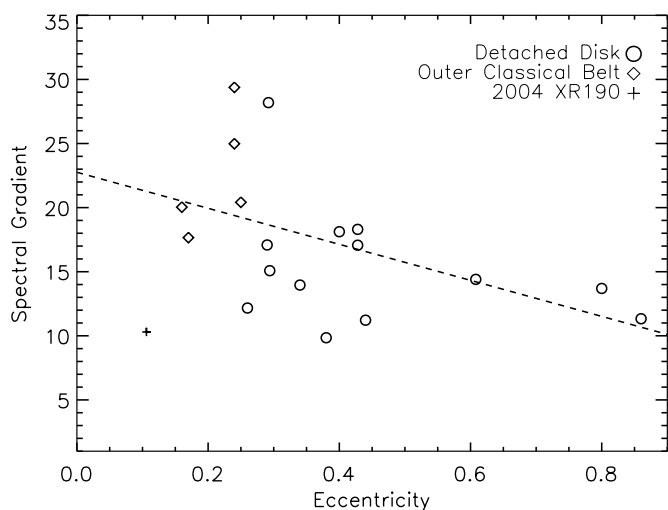


Figure 7. Eccentricity vs. the spectral gradient for 2004 XR₁₉₀, detached disk, and outer classical belt objects. There appears to be a trend that the lower the eccentricity the redder the object, but since there is only a few objects in the sample this trend is only at the 97% confidence level using the Pearson correlation coefficient. The lower eccentricity outer classical belt objects (diamonds) are near the ultra-red spectral gradient region while the higher eccentricity detached disk objects (circles) are mostly moderately red to neutral in color. 2004 XR₁₉₀ is dynamically distinct (see the text) but has been simulated as a detached disk object by Gomes et al. (2008) and thus is plotted for completeness (plus sign). A linear fit is shown by the dashed line.

To compare the spectral gradients of outer classical belt objects with the low inclination “cold” classical belt objects the Student’s *t*-test and the K–S test were performed on the two populations (Figure 5). The two distributions do not appear to be significantly different ($< 2\sigma$) and thus could come from the same parent population (Table 6). This is unlike the detached and strict scattered disks which have $> 3\sigma$ confidence in the differences of their spectral gradient distributions when compared to the low inclination “cold” classical belt objects (Table 6). Thus the detached disk and strict scattered disk objects are unlikely to have come from the same parent population as the low inclination “cold” classical belt objects.

Table 6 shows that the K–S test hints at a possible trend with there being significant differences between the outer classical belt spectral gradient distribution and the strict scattered and detached disk objects but with only five known outer classical belt objects the test is unreliable. About twice as many outer classical belt objects need to be discovered and have their spectral gradients determined in order to confirm or reject them as having significantly different spectral gradients from the various dynamical populations in the outer solar system. It is apparent that the outer classical belt objects are very red objects and they are redder than both the detached disk and strict scattered disk, and less red than the low inclination “cold” classical KBOs.

As shown in Figure 5, the colors of the scattered disk objects not in resonances are the least red. The detached disk objects are slightly redder while the outer classical belt objects are even redder and finally the low inclination “cold” classical KBOs are the reddest objects. The high-order resonance objects appear to span most of the spectral gradient range of the various populations (Figure 6). The significant differences in spectral gradients for some of the populations are likely because the objects come from different source regions. It is also possible that the differences in the spectral gradients of the various populations come from significantly different surface

Table 7
Pearson Correlations for Spectral Gradients and Dynamics

Parameter 1 ^a	Parameter 2 ^a	N^b	r_{corr}^c	Sig ^d
$S(\text{Det,Out,ScatStr,LowIncl})$	e	53	−0.80	99.99%
$S(\text{Det,Out,ScatStr})$	e	25	−0.53	99.1%
$S(\text{Det,Out,ScatStr,HighRes})$	e	35	−0.41	98.5%
$S(\text{Det,Out})$	e	18	−0.49	97%
$S(\text{Det,Out,ScatStr})$	q	25	0.39	85%
$S(\text{Det,Out})$	q	18	−0.18	60%
$S(\text{Det,Out,ScatStr})$	i	25	0.06	20%
$S(\text{Det,Out})$	i	18	−0.03	0%

Notes.

^a The two parameters being compared through the Pearson correlation coefficient. S is the spectral gradient with the dynamical groups used in parentheses where Det is the detached disk, Out is the outer main belt, ScatStr is the scattered strict, LowIncl is the low inclination “cold” classical belt, and HighRes is the high-order Neptune resonance objects.

^b The number of objects used in the correlation.

^c r_{corr} is the Pearson correlation coefficient.

^d Sig is the confidence of significance of the correlation.

weathering processes on the objects over the age of the solar system, such as different collisional or sublimation histories. It is apparent that the objects more distant from the Sun are on average redder.

4.3. Spectral Gradients Versus Orbital Dynamics

To further explore the origins of the detached disk and outer classical belt objects, their eccentricities versus spectral gradient were plotted (Figure 7). There is an apparent trend that the lower the eccentricity the redder the object. The Pearson correlation coefficient is -0.49 using the 18 known spectral gradients of the detached disk and outer classical belt objects. The correlation with eccentricity is only significant at about the 97% level and additional low eccentricity outer classical belt objects need to be found to confirm or reject this possible trend (Table 7). Including the strict scattered disk objects increases the significance of the correlation with eccentricity to 99.1%. If the low inclination “cold” main classical KBOs are also included, the trend is even stronger with a Pearson correlation coefficient of -0.80 and a significance at the 99.99% confidence limit (Figure 8). There is no trend of spectral gradient with the inclination or perihelion distances of the detached disk and outer classical belt objects (Table 7). Including the strict scattered disk also finds no trend with spectral gradient and inclination or perihelion distance.

5. SUMMARY

Thirty-three extreme outer solar system objects were observed to determine their optical colors.

1. The three possible inner Oort Cloud objects (Sedna, 2006 SQ₃₇₂, and 2000 OO₆₇) all have ultra-red surfaces (spectral gradient $S \sim 25$). These ultra-red surfaces are abundant in the low inclination “cold” classical KBO population and is believed to be associated with organic-rich material. Because the ultra-red material is only seen in the very outer parts of the observable solar system, it is likely that this material has not been significantly thermally altered. The red lobe of the Centaur distribution could thus either be from the low inclination classical KBO population or from the inner Oort Cloud population.
2. For the first time, a systematic color determination of extended or detached disk objects was obtained. Most

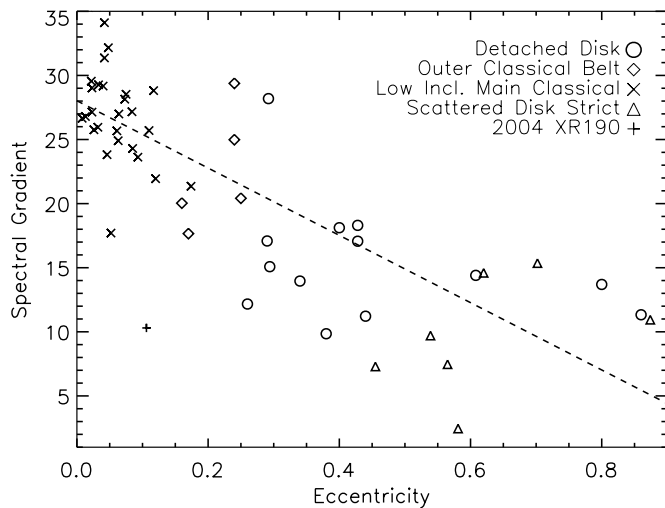


Figure 8. Same as Figure 7 except now the scattered disk objects not in high-order resonances (triangles) and the low inclination “cold” main classical KBOs (X’s) have been added. Adding these objects strengthens the trend that lower eccentricity objects have redder colors and is at the 99.99% confidence level.

detached disk objects have only moderately red surfaces ($10 \lesssim S \lesssim 18$). Though slightly redder on average than the scattered disk, the detached disk colors are consistent with being from the same source region as the scattered disk objects. The only ultra-red objects observed with scattered disk-like orbits appear to be objects in high-order resonances with Neptune.

3. The outer classical KBOs, which have semimajor axes beyond the 2:1 resonance with Neptune and low eccentricities, were found to be very red ($S \gtrsim 20$) and are on average redder than the detached disk objects. Unlike the scattered disk and detached disk, the outer classical belt objects have spectral gradients similar to the ultra-red low inclination “cold” classical KBOs though they appear to be less red on average.
4. The two retrograde objects with perihelia in the outer solar system (2008 KV₄₂ and 2008 YB₃) and the extremely high inclination object (127546) 2002 XU₉₃ show only moderately red colors ($S \sim 9$). These colors are very similar to the known comets, dead comets, damocloids, Jupiter Trojans, Neptune Trojans, irregular satellites, D-type main belt asteroids, scattered disk objects, and the neutral lobe of the Centaurs. 2008 YB₃ perihelion is near Jupiter; thus this object has had its surface thermally altered over the age of the solar system as is probably true for all the above moderately red populations. 2008 KV₄₂ has a rather large perihelion at 21 AU and it is unknown if it has ever approached closer to the Sun. The moderately red surface color suggests its surface has likely been thermally altered.
5. The detached disk and outer classical KBOs show a trend that the lower the eccentricity the redder the object. This trend is currently not statistically significant since only a few of these objects are known. The trend is strengthened when adding the strict scattered disk and low inclination “cold” classical KBOs. The trend must be confirmed through discovering and measuring the colors of more outer classical belt objects.

I thank Chadwick A. Trujillo and Henry H. Hsieh for helpful comments that improved this manuscript. This paper includes data gathered with the 6.5 m Magellan telescopes located at

Las Campanas Observatory, Chile. This work is based in part on data collected with the Subaru telescope, which is operated by the National Astronomical Observatory of Japan. This work was partially supported by the National Aeronautics and Space Administration through the NASA Astrobiology Institute (NAI) under Cooperative Agreement No. NNA04CC09A issued to the Carnegie Institution of Washington.

REFERENCES

- Allen, R., Bernstein, G., & Malhotra, R. 2001, *ApJ*, **549**, L241
- Allen, R., Gladman, B., Kavelaars, J., Petit, J., Parker, J., & Nicholson, P. 2006, *ApJ*, **640**, L83
- Barucci, M. A., Belskaya, I., Fulchignoni, M., & Birlan, M. 2005a, *AJ*, **130**, 1291
- Barucci, M. A., Brown, M., Emery, J., & Merlin, F. 2008, in *The Solar System Beyond Neptune*, ed. M. Barucci, H. Boehnhardt, D. Cruikshank, & A. Morbidelli (Tucson, AZ: Univ. Arizona Press), 143
- Barucci, M. A., Cruikshank, D., Dotto, E., Merlin, F., Poulet, F., Dalle Ore, C., Fornasier, S., & de Bergh, C. 2005b, *A&A*, **439**, L1
- Bauer, J., Meech, K., Fernandez, Y., Pittichova, J., Hainaut, O., Boehnhardt, H., & Delsanti, A. 2003, *Icarus*, **166**, 195
- Becker, A., et al. 2008, *ApJ*, **682**, L53
- Brasser, R. 2008, *A&A*, **492**, 251
- Brasser, R., Duncan, M., & Levison, H. 2006, *Icarus*, **184**, 59
- Brown, M., Trujillo, C., & Rabinowitz, D. 2004, *ApJ*, **617**, 645
- Cruikshank, D., Imanaka, H., & Dalle Ore, C. 2005, *Adv. Space Res.*, **36**, 178
- de Bergh, C., Schmitt, B., Moroz, L., Quirico, E., & Cruikshank, D. 2008, in *The Solar System Beyond Neptune*, ed. M. Barucci, H. Boehnhardt, D. Cruikshank, & A. Morbidelli (Tucson, AZ: Univ. Arizona Press), 483
- Delsanti, A., Boehnhardt, H., Barrera, L., Meech, K., Sekiguchi, T., & Hainaut, O. 2001, *A&A*, **380**, 347
- DeMeo, F., et al. 2009, *A&A*, **493**, 283
- Doressoundiram, A., Barucci, M. A., Romon, J., & Veillet, C. 2001, *Icarus*, **154**, 277
- Doressoundiram, A., Boehnhardt, H., Tegler, S., & Trujillo, C. 2008, in *The Solar System Beyond Neptune*, ed. M. Barucci, H. Boehnhardt, D. Cruikshank, & A. Morbidelli (Tucson, AZ: Univ. Arizona Press), 91
- Doressoundiram, A., Peixinho, N., Doucet, C., Mousis, O., Barucci, M. A., Petit, J., & Veillet, C. 2005, *Icarus*, **174**, 90
- Doressoundiram, A., Peixinho, N., Moullet, A., Fornasier, S., Barucci, M. A., Beuzit, J., & Veillet, C. 2007, *AJ*, **134**, 2186
- Doressoundiram, A., Tozzi, G., Barucci, M., Boehnhardt, H., Fornasier, S., & Romon, J. 2003, *AJ*, **125**, 2721
- Doressoundiram, A., et al. 2002, *AJ*, **124**, 2279
- Duncan, M. 2008, *Space Sci. Rev.*, **138**, 109
- Duncan, M., Brasser, R., Dones, L., & Levison, H. 2008, in *The Solar System Beyond Neptune*, ed. M. Barucci, H. Boehnhardt, D. Cruikshank, & A. Morbidelli (Tucson, AZ: Univ. Arizona Press), 315
- Duncan, M., & Levison, H. 1997, *Science*, **276**, 1670
- Duncan, M., Levison, H., & Budd, S. 1995, *AJ*, **110**, 3073
- Duncan, M., Levison, H., & Dones, L. 2004, in *Comets II*, ed. M. Festou, H. Keller, & H. Weaver (Tucson, AZ: Univ. Arizona Press), 193
- Elliot, J., et al. 2005, *AJ*, **129**, 1117
- Emel’yanenko, V., Asher, D., & Bailey, M. 2003, *MNRAS*, **338**, 443
- Emel’yanenko, V., & Kiseleva, E. 2008, *Astron. Lett.*, **34**, 271
- Emery, J., Dalle Ore, C., Cruikshank, D., Fernandez, Y., Trilling, D., & Stansberry, J. 2007, *A&A*, **466**, 395
- Fitzsimmons, A., Dahlgren, M., Lagerkvist, C., Magnusson, P., & Williams, I. 1994, *A&A*, **282**, 634
- Fornasier, S., Dotto, E., Hainaut, O., Marzari, F., Boehnhardt, H., de Luise, F., & Barucci, M. A. 2007, *Icarus*, **190**, 622
- Fulchignoni, M., Belskaya, I., Barucci, M. A., De Sanctis, M., & Doressoundiram, A. 2008, in *The Solar System Beyond Neptune*, ed. M. Barucci, H. Boehnhardt, D. Cruikshank, & A. Morbidelli (Tucson, AZ: Univ. Arizona Press), 181
- Gallardo, T. 2006, *Icarus*, **181**, 205
- Gladman, B., & Collin, C. 2006, *ApJ*, **643**, L135
- Gladman, B., Holman, M., Grav, T., Kavelaars, J., Nicholson, P., Aksnes, K., & Petit, J. 2002, *Icarus*, **157**, 269
- Gladman, B., Marsden, B., & VanLaerhoven, C. 2008, in *The Solar System Beyond Neptune*, ed. M. Barucci, H. Boehnhardt, D. Cruikshank, & A. Morbidelli (Tucson, AZ: Univ. Arizona Press), 43
- Gladman, B., et al. 2009, *ApJ*, **697**, L91
- Gomes, R. 2003, *Icarus*, **161**, 404

- Gomes, R., Fernandez, J., Gallardo, T., & Brunini, A. 2008, in *The Solar System Beyond Neptune*, ed. M. Barucci, H. Boehnhardt, D. Cruikshank, & A. Morbidelli (Tucson, AZ: Univ. Arizona Press), 259
- Gomes, R., Gallardo, T., Fernandez, J., & Brunini, A. 2005, *Celest. Mech. Dyn. Astron.*, 91, 109
- Gradie, J., & Veverka, J. 1980, *Nature*, 283, 840
- Grav, T., & Bauer, J. 2007, *Icarus*, 191, 267
- Grav, T., Holman, M., & Fraser, W. 2004, *ApJ*, 613, L77
- Grav, T., Holman, M. J., Gladman, B. J., & Aksnes, K. 2003, *Icarus*, 166, 33
- Grundy, W. 2009, *Icarus*, 199, 560
- Gulbis, A., Elliot, J., & Kane, J. 2006, *Icarus*, 183, 168
- Hahn, J., & Malhotra, R. 2005, *AJ*, 130, 2392
- Hainaut, O., & Delsanti, A. 2002, *A&A*, 389, 641
- Ida, S., Larwood, J., & Burkett, A. 2000, *ApJ*, 528, 351
- Jewitt, D. 2002, *AJ*, 123, 1039
- Jewitt, D. 2005, *AJ*, 129, 530
- Jewitt, D., & Luu, J. 2001, *AJ*, 122, 2099
- Jewitt, D., Luu, J., & Trujillo, C. 1998, *AJ*, 115, 2125
- Jewitt, D., Peixinho, N., & Hsieh, H. 2007, *AJ*, 134, 2046
- Kaib, N., & Quinn, T. 2009, *Science*, 325, 1234
- Kaib, N., et al. 2009, *ApJ*, 695, 268
- Karlsson, O., Lagerkvist, C., & Davidsson, B. 2009, *Icarus*, 199, 106
- Kavelaars, J., Jones, L., Gladman, B., Parker, J., & Petit, J. 2008, in *The Solar System Beyond Neptune*, ed. M. Barucci, H. Boehnhardt, D. Cruikshank, & A. Morbidelli (Tucson, AZ: Univ. Arizona Press), 59
- Kavelaars, J., et al. 2009, *AJ*, 137, 4917
- Kenyon, S., & Bromley, B. 2004, *Nature*, 432, 598
- Kenyon, S., Bromley, B., O'Brien, D., & Davis, D. 2008, in *The Solar System Beyond Neptune*, ed. M. Barucci, H. Boehnhardt, D. Cruikshank, & A. Morbidelli (Tucson, AZ: Univ. Arizona Press), 293
- Lamy, P., & Toth, I. 2009, *Icarus*, 201, 674
- Leto, G., Jakubik, M., Paulech, T., Neslusan, L., & Dbyczynski, P. 2008, *MNRAS*, 391, 1350
- Levison, H., & Duncan, M. 1997, *Icarus*, 127, 13
- Levison, H., Duncan, M., Dones, L., & Gladman, B. 2006, *Icarus*, 184, 619
- Levison, H., & Morbidelli, A. 2003, *Nature*, 426, 419
- Levison, H., Morbidelli, A., Vanlaerhoven, C., Gomes, R., & Tsiganis, K. 2008, *Icarus*, 196, 258
- Lykawka, P., & Mukai, T. 2007a, *Icarus*, 189, 213
- Lykawka, P., & Mukai, T. 2007b, *Icarus*, 192, 238
- Malhotra, R. 1995, *AJ*, 110, 420
- Meech, K., et al. 2009, *Icarus*, 201, 719
- Melita, M., Licandro, J., Jones, D., & Williams, I. 2008, *Icarus*, 195, 686
- Miyazaki, S., et al. 2002, *PASJ*, 54, 833
- Morbidelli, A., & Levison, H. 2004, *AJ*, 128, 2564
- Morbidelli, A., Levison, H., & Gomes, R. 2008, in *The Solar System Beyond Neptune*, ed. M. Barucci, H. Boehnhardt, D. Cruikshank, & A. Morbidelli (Tucson, AZ: Univ. Arizona Press), 275
- Nesvorny, D., & Roig, F. 2001, *Icarus*, 150, 104
- Oort, J. 1950, *Bull. Astron. Inst. Neth.*, 11, 91
- Peixinho, N., Boehnhardt, H., Belskaya, I., Doressoundiram, A., Barucci, M., & Delsanti, A. 2004, *Icarus*, 170, 153
- Peixinho, N., Doressoundiram, A., Delsanti, A., Boehnhardt, H., Barucci, M. A., & Belskaya, I. 2003, *A&A*, 410, L29
- Peixinho, N., Lacerda, P., & Jewitt, D. 2008, *AJ*, 136, 1837
- Petit, J., Morbidelli, A., & Valsecchi, G. 1999, *Icarus*, 141, 367
- Ragozzine, D., & Brown, M. 2007, *AJ*, 134, 2160
- Roig, F., Ribeiro, A., & Gil-Hutton, R. 2008, *A&A*, 483, 911
- Santos-Sanz, P., Ortiz, J., Barrera, L., & Boehnhardt, H. 2009, *A&A*, 494, 693
- Schwamb, M., Brown, M., & Rabinowitz, D. 2009, *ApJ*, 694, L45
- Sheppard, S., & Trujillo, C. 2006, *Science*, 313, 511
- Smith, J., et al. 2002, *AJ*, 123, 2121
- Smith, J., et al. 2005, *BAAS*, 37, 1379
- Snodgrass, C., Lowry, S., & Fitzsimmons, A. 2008, *MNRAS*, 385, 737
- Stern, A. 2003, *Nature*, 424, 639
- Tegler, S., Bauer, J., Romanishin, W., & Peixinho, N. 2008, in *The Solar System Beyond Neptune*, ed. M. Barucci, H. Boehnhardt, D. Cruikshank, & A. Morbidelli (Tucson, AZ: Univ. Arizona Press), 105
- Tegler, S., & Romanishin, W. 1998, *Nature*, 392, 49
- Tegler, S., & Romanishin, W. 2000, *Nature*, 407, 979
- Tegler, S., & Romanishin, W. 2003, *Icarus*, 161, 181
- Thomas, F., & Morbidelli, A. 1996, *Celest. Mech. Dyn. Astron.*, 64, 209
- Trujillo, C., & Brown, M. 2002, *ApJ*, 566, L125
- Trujillo, C., Jewitt, D., & Luu, J. 2001, *AJ*, 122, 457
- Vilas, F., & Smith, B. 1985, *Icarus*, 64, 503